MATERIALS CHEMISTRY FRONTIERS

RESEARCH ARTICLE

View Article Online
View Journal | View Issue

Cite this: *Mater. Chem. Front.*, 2025, **9**, 3219

Optimizing combination between thianthrene and benzophenone toward efficient room-temperature phosphorescence and oxygen sensing

Zhiqiang Yang, Meng Liu, Yunpeng Ge, Yingbo Lv, Zhe Feng, Haichao Liu* and Bing Yang*

Received 29th July 2025,
Accepted 12th September 2025

DOI: 10.1039/d5qm00556f

rsc.li/frontiers-materials

Purely organic room-temperature phosphorescence (RTP) materials show broad prospects for various applications due to their characteristics such as stimuli-responsiveness and high exciton utilization. A key challenge for improving the performance of purely organic RTP materials lies in suppressing non-radiative decay while enhancing spin–orbit coupling (SOC). To this end, we systematically combined benzophenone (BP) with thianthrene (TA) at different modification sites and with varying numbers of substituents, creating a class of high-efficiency RTP materials by leveraging the folded conformation of TA groups and introducing intramolecular charge transfer (ICT) to enhance SOC. Benefiting from the separated fluorescence–RTP dual emission of these materials, highly sensitive ratiometric optical oxygen sensing can be achieved with a Stern–Volmer coefficient of up to 10.65 kPa^{-1}. This study not only deepens the understanding of the structure–property relationship of TA-based RTP materials but also provides an effective strategy for performance enhancement and functional development of purely organic RTP materials.

Introduction

Purely organic RTP materials have exhibited great potential for applications in sensing,[1–3] bio-imaging,[4–6] anti-counterfeiting,[7–9] information encryption,[10–12] and photoelectric devices[13–15] due to their typical characteristics, such as stimuli-responsiveness,[10] long lifetimes,[6] and high exciton utilization.[13] Phosphorescence arises from radiative decay between states of different spin multiplicities, typically occurring between the first excited triplet state (T_1) and the ground singlet state (S_0).[16] In principle, transitions between the states of different spins are forbidden, so that the T_1 excited state cannot be populated by direct absorption of light. Instead, the population of the T_1 excited state relies on intersystem crossing (ISC), a process in which the system transitions from excited singlet states to excited triplet states.[17] In recent years, there has been a surge of interest in the rational design and theoretical study of organic RTP molecules, aiming to achieve well-behaved RTP materials with high phosphorescence efficiency (ϕ_P) and long lifetimes.[18,19] Correspondingly, two primary strategies have been widely adopted: (i) internally, incorporating non-metallic heavy atoms (*e.g.*, Br, I and Se) or heteroatoms (*e.g.*, B, O, N, and S) into molecular skeletons to enhance SOC, thereby promoting efficient ISC[20–22] and (ii) externally, providing rigid environments, such as through crystallization,[23] H-aggregation,[24] or embedding in a host matrix,[25] to minimize non-radiative deactivation pathways and increase the efficiency of triplet radiative decay. In a sense, promoting SOC is a more fundamental scientific issue for the study of purely organic RTP materials, compared to simply suppressing non-radiative decay of the triplet excitons.[16] This promotion, driven by rational molecular design and precise chemical modification, not only facilitates the development of efficient, purely organic RTP materials but also promises to unlock the discovery of novel materials, drive original conceptual innovation, and enable targeted applications.[26–29]

Thianthrene (TA), an intriguing sulfur-containing heterocyclic molecule exhibiting efficient RTP, has emerged as a distinctive molecular system within the field of RTP materials.[30,31] Its RTP arises from enhanced SOC achieved through a folded conformation.[32] In essence, as the molecular folding degree increases, the non-bonding n orbitals of sulfur atoms progressively decouple from the π molecular orbitals of the TA molecule, leading to a substantial enhancement of SOC (approximately 1–2 orders of magnitude) compared to the planar conformation.[20,33] Furthermore, the considerable potential of TA-based RTP

State Key Laboratory of Supramolecular Structure and Materials, College of Chemistry, Jilin University, Changchun, China. E-mail: hcliu@jlu.edu.cn, yangbing@jlu.edu.cn

derivatives has been explored for applications such as ratiometric optical oxygen sensing.[2,3,34] The ratiometric measurement method overcomes the limitations of direct intensity measurement that are susceptible to instrument fluctuation, scattered light, and possible photobleaching of indicator dyes.[35,36] This advantageous application potential can be ascribed to the dual emission of fluorescence and RTP typically observed in the mono-dispersed state of TA-based derivatives. Nevertheless, our understanding of TA remains incomplete, particularly regarding structural modifications and the tunable potential of its photophysical and oxygen-sensing properties.

Benzophenone (BP) as a prototypical example is positively employed as a building block in the design of RTP molecules due to its high ISC efficiency close to unity, which is expected to improve RTP properties.[37–39] Moreover, compared to the TA unit, the BP unit exhibits weak acceptor properties. Its combination with TA is expected to introduce intramolecular charge transfer (ICT), synergistically enhancing SOC to improve the RTP properties of TA-based derivatives. TA possesses two common modification sites, 1- and 2-positions, and the different modification sites may exert a certain effect on the resulting RTP properties.[40] Therefore, it is expected to be useful in a rational chemical modification strategy to achieve well-behaved RTP materials. In this work, we systematically investigate the combination of BP and TA, focusing on optimizing both the modification site and the number of substituents. Our finding reveals that when BP is combined with TA at the 1-position, the resulting molecules predominantly show single emission of RTP. Conversely, when BP is combined with TA at the 2-position, the resulting molecules exhibit a dual emission of fluorescence and efficient RTP. When BP is combined with two TA at the 2-position, the resulting molecule exhibits improved RTP performance. This is primarily attributed to three factors: firstly, the attachment of BP with two TA groups at the 2-position leads to a denser distribution of excited state energy levels, thus creating more potential ISC pathways; secondly, the folded structure of TA and moderate ICT result in a suitable enhancement of SOC; thirdly, 2-position substitution of TA significantly reduced the SOC between the T_1 and S_0 states compared to 1-position substitution. These three factors collectively accelerate the ISC process while simultaneously preventing excessive SOC from causing non-radiative deactivation of triplet excitons. Finally, the potential application of the 2TA–BP–2TA molecule, which features a dual emission of fluorescence and highly efficient RTP, was investigated for ratiometric optical oxygen sensing and detection. This successfully achieved highly sensitive oxygen sensing with a Stern–Volmer coefficient (K_{SV}) of up to 10.65 kPa^{-1}. This work not only provides a better understanding of the structure–property relationship of TA-based RTP materials, but also suggests a feasible chemical modification strategy to improve the key performance of purely organic RTP materials.

Results and discussion

As shown in Scheme 1, four compounds are designed in terms of both the modification site of TA and the number of TA units, including phenyl(4-(thianthren-1-yl)phenyl)methanone (1TA–BP), bis(4-(thianthren-1-yl)phenyl)methanone (1TA–BP–1TA), phenyl(4-(thianthren-2-yl)phenyl)methanone (2TA–BP), and bis(4-(thianthren-2-yl)phenyl)methanone (2TA–BP–2TA). All these compounds were successfully synthesized *via* Suzuki coupling reactions. The detailed synthetic procedures can be found in the SI. The structural characterization of these compounds was carried out using ^{1}H NMR, ^{13}C NMR, mass spectrometry, and single-crystal X-ray diffraction (SCXRD).

As shown in Fig. S2–S5, we first conducted fundamental photophysical characterization of these four compounds in dilute solution (10^{-5} M). The results reveal that TA substitution at the 2-position induces a more pronounced redshift in the absorption spectra compared to substitution at the 1-position. Regarding emission characteristics, all four molecules exhibit single-band fluorescence. Notably, their photoluminescence (PL) spectra exhibit a progressive redshift with increasing solvent polarity, clearly demonstrating the presence of ICT characteristics. Given that the TA molecule is characterized by a folded conformation, we then perform an investigation on the

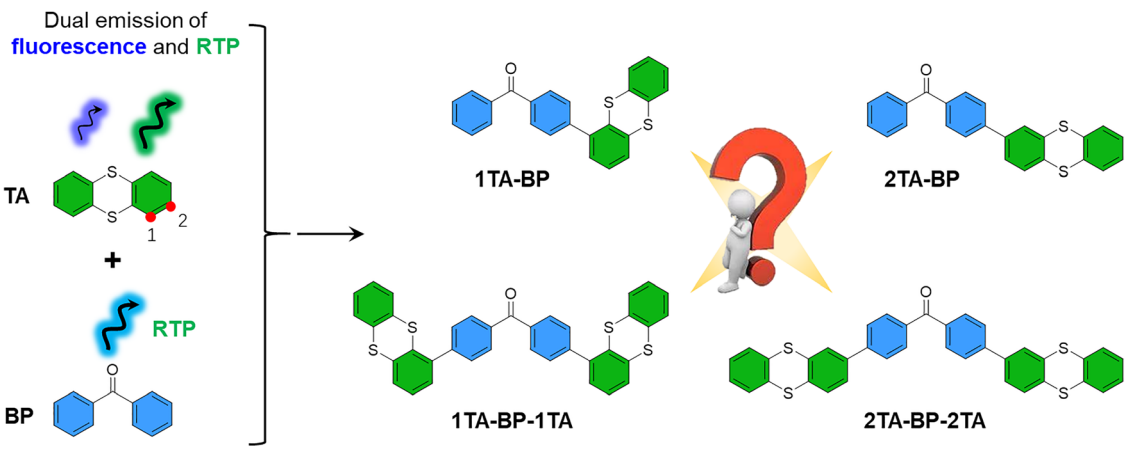

Scheme 1 Design of highly efficient RTP materials *via* the combination of TA and BP.

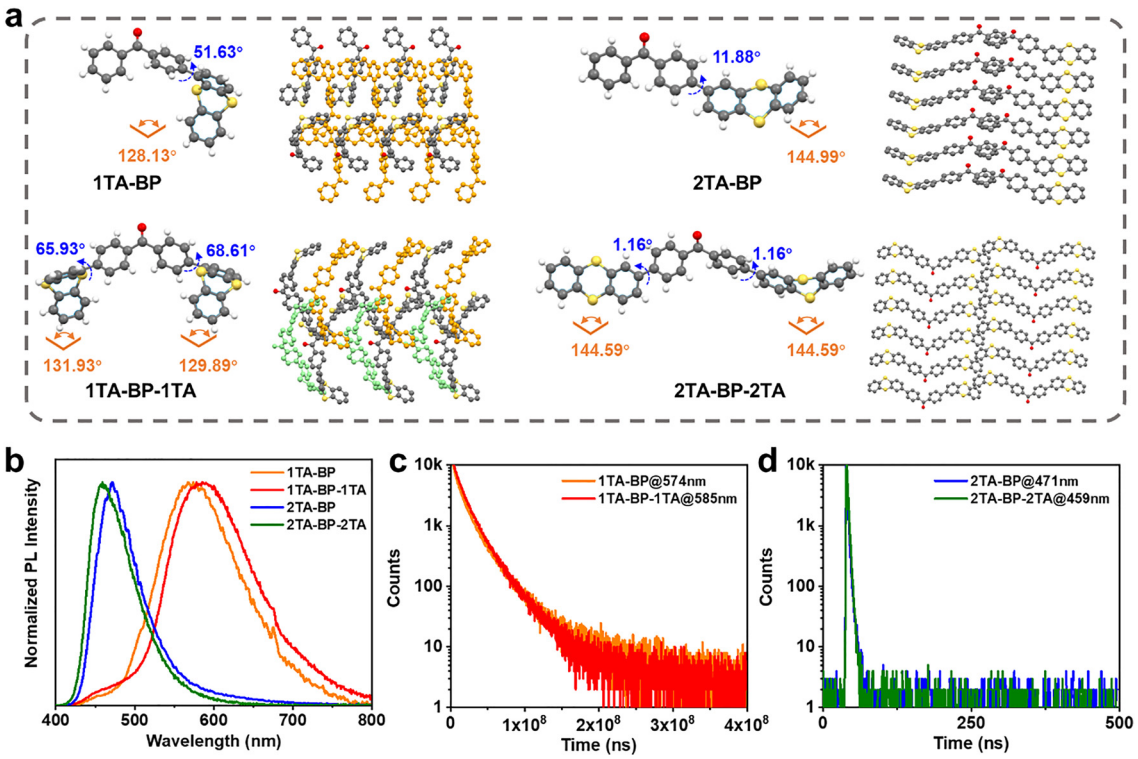

Fig. 1 (a) Geometric and packing characteristics of 1TA–BP, 1TA–BP–1TA, 2TA–BP, and 2TA–BP–2TA in their crystalline states. (b) Steady-state PL spectra of the1TA–BP, 1TA–BP–1TA, 2TA–BP, and 2TA–BP–2TA crystals. PL decay profiles of (c) 1TA–BP and 1TA–BP–1TA crystals and (d) 2TA–BP and 2TA–BP–2TA crystals at their respective emission peaks.

molecular geometries and packing motifs of the studied compounds in the crystals. Single crystals of 1TA–BP, 1TA–BP–1TA, and 2TA–BP were successfully grown *via* the solvent diffusion method using a mixture of chloroform and methanol solvents, whereas 2TA–BP–2TA single crystals were obtained through a sublimation method under reduced pressure. Then, their crystal structures were determined through SCXRD. As shown in Fig. 1a, two distinct structural characteristics emerge from comparative analysis of molecular geometries. On the one hand, the substitution position of TA units on the BP unit significantly influences molecular planarity: 1-position substitution induces substantial torsional angles between aromatic planes (51.63° for 1TA–BP; 65.93° and 68.61° for 1TA–BP–1TA), resulting in a highly twisted conformation. In contrast, the combination between 2-position TA and BP induces a small twisted angle (11.88° for 2TA–BP, and 1.16° for 2TA–BP–2TA), which makes molecules maintain a nearly linear or coplanar conformation. The conformational dependence on the substitution position of TA in combination with BP originates from enhanced steric hindrance at the 1-position. On the other hand, the folded angle of the TA units in these studied compounds is different. The TA units in 1TA–BP (128.13°) and 1TA–BP–1TA (131.93° and 129.89°) exhibit a smaller folded angle compared to those in 2TA–BP (144.99°) and 2TA–BP–2TA (144.59°). This divergence correlates with conjugation effects, that is, the enhanced planarity in 2-substituted derivatives facilitates extended π-conjugation, as revealed by the small twisted angle between 2-position TA and BP units. These results rationalize the absorption redshift induced by 2-position TA substitution. Consequently, 1TA–BP and 1TA–BP–1TA molecules in the crystals exhibit an interwoven stacking structure, while 2TA–BP and 2TA–BP–2TA display ordered, one-dimensional long-range stacking. This structural dichotomy underscores the critical role of the substitution position in modulating both the molecular conformation and supramolecular organization.

PL analysis of the four crystalline compounds reveals distinct emission profiles governed by substitution patterns. While all these four studied compounds display a single emission band, a pronounced wavelength difference can be observed (Fig. 1b). 1TA–BP and 1TA–BP–1TA crystals show a long-wavelength emission band peaking at 574 nm and 585 nm, respectively, while 2TA–BP and 2TA–BP–2TA crystals exhibit a significantly blue-shifted emission maxima at 471 nm and 459 nm, respectively. Transient PL spectra further resolve the mechanism of the emission profiles. The 1TA-substituted systems demonstrate a long-lived excited-state character with millisecond-scale lifetimes (26.45 ms for 1TA–BP; 20.87 ms for 1TA–BP–1TA), consistent with phosphorescence behavior (Fig. 1c). In stark contrast, 2TA-substituted analogues show nanosecond-scale lifetimes (2.56 ns for 2TA–BP; 2.37 ns for 2TA–BP–2TA), characteristic of fluorescence (Fig. 1d). As established in the crystallographic analysis, these structure–property relationships underscore the critical role of molecular geometry in tuning optoelectronic behavior.

Building upon prior findings by our group, TA-based derivatives in their aggregate states generally show weak and even no RTP due to aggregation-caused RTP quenching.[10] To clarify the correlation between the molecular structure and RTP properties, we further disperse these four compounds in a poly(methyl methacrylate) (PMMA) matrix. The UV-Vis spectra of the 1.00 wt% doped PMMA films are similar to those in the solution state, indicating that the molecules in the films predominantly exist in a monodispersed state (Fig. S6). Subsequently, steady-state and transient PL spectra for these four compounds in the films were recorded under both ambient and deoxygenated (vacuum) conditions. In air, PMMA films doped with 1TA–BP and 1TA–BP–1TA display very faint emission bands spanning 400 nm to 700 nm. Their millisecond-scale lifetimes confirm their RTP nature, which aligns with phenomena observed in their crystals. Upon transfer to a vacuum environment, a dramatic enhancement in their emission intensity was observed, with peaks at 513 nm and 503 nm, along with corresponding lifetimes of 32.60 ms and 20.42 ms, and ϕ_P values were measured to be 4.8% and 7.9%, respectively (Fig. 2a and c). To exclude the potential for thermally activated delayed fluorescence (TADF), temperature-dependent PL and transient PL spectroscopic characterization was additionally conducted on the PMMA films doped with 1TA–BP and 1TA–BP–1TA. Both the decrease in steady-state emission intensity with increasing temperature and the monotonic shortening of lifetimes further validated their RTP nature (Fig. S7 and S8). Diverging from 1TA–BP and 1TA–BP–1TA, the doped PMMA films of 2TA–BP and 2TA–BP–2TA presented a well-defined single emission peak in air, located at 470 nm and 473 nm, respectively. With lifetimes of 5.21 ns and 5.10 ns, these emissions are assignable to fluorescence. When placed in a vacuum, these two films displayed new, dominant emission bands at longer wavelengths, with peaks observed at 545 nm and 552 nm, respectively. Their long lifetimes of 56.29 ms and 55.68 ms are indicative of the existence of RTP (Fig. 2b and d). Interestingly, 2-position-substituted TA systems exhibit much higher ϕ_P values than 1-position-substituted TA systems (with 2TA–BP at 17.9% and 2TA–BP–2TA at 31.3%). Moreover, dual TA substitution enhances ϕ_P values significantly compared to single-TA-functionalized systems (Table 1).

It is intriguing that such structurally similar molecules exhibit vast differences in their luminescence performance. To elucidate this, employing their determined geometries in crystals, we conducted a systematic investigation into their excited-state properties using time-dependent density functional theory (TD-DFT). Energy level analysis reveals that substitution at the 2-position of TA, compared to substitution at the 1-position, induces a decrease in energy levels (Fig. S9). This energy lowering is expected to result in a redshift of the RTP emission, which is consistent with the experimental observations. Based on Kasha's rule, we focused our investigation on the photophysical processes of the lowest excited state.[41] As a decisive factor for the ISC rate, we systematically calculated the SOC coefficients for T_1–S_0 and from S_1–T_1 up to S_1–T_{10}. The results indicate that all these systems exhibit high SOC coefficients, confirming their excellent characteristics for efficient triplet exciton generation (Fig. 3a). However, TA substitution at the 1-position significantly enhances the SOC effect compared to substitution at the 2-position. While this enhancement is beneficial for the conversion from singlet excitons to triplet excitons, it simultaneously leads to a substantial increase in the $T_1 \rightarrow S_0$ ISC (the SOC coefficient between T_1 and S_0 was calculated up to 61.54 cm^{-1} for 1TA–BP and 60.29 cm^{-1} for 1TA–BP–1TA), consequently inducing a more intense non-radiative transition process. This dual effect can reasonably

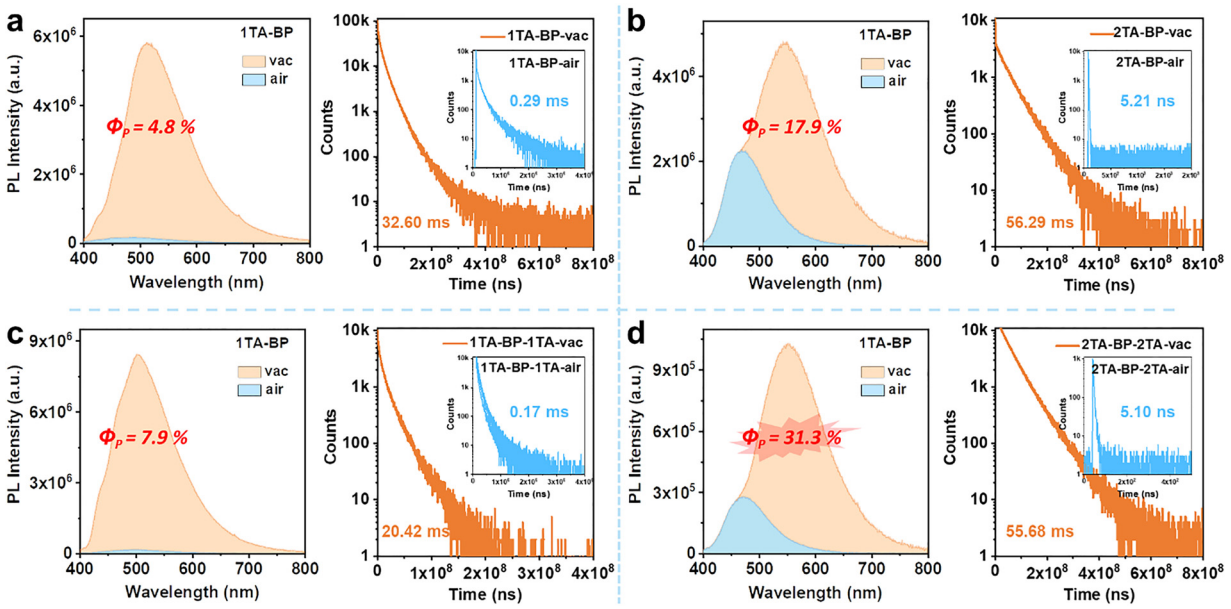

Fig. 2 Steady-state PL spectra (filled blue for air and filled yellow for vacuum) and PL decay profiles (blue for air and yellow for vacuum) of the PMMA films doped with (a) 1TA–BP, (b) 2TA–BP, (c) 1TA–BP–1TA, and (d) 2TA–BP–2TA, measured in both air and vacuum.

Table 1 Key photophysical parameters of 1TA–BP, 2TA–BP, 1TA–BP–1TA, and 2TA–BP–2TA

Compound	λ_F (nm)	$\lambda_P{}^a$ (nm)	τ_F (ns)	$\tau_P{}^a$ (ms)	ϕ_F (%)	$\phi_P{}^{ab}$ (%)
1TA–BP	—	513	—	32.60	—	4.8
2TA–BP	470	545	5.21	56.29	7.0	17.9
1TA–BP–1TA	—	503	—	20.42	—	7.9
2TA–BP–2TA	473	552	5.10	55.68	6.9	31.3

λ_F: fluorescence peak position, λ_P: phosphorescence peak position, τ_F: fluorescence lifetime, τ_P: phosphorescence lifetime, ϕ_F: fluorescence quantum yield, and ϕ_P: RTP quantum yield. [a] Measurement results obtained under deoxygenated conditions. [b] Calculated results based on measurements before and after deoxygenation at room temperature.

explain the experimentally observed phenomena: although the 1-position substituted systems exhibit pure RTP emission characteristics, their RTP efficiencies are generally lower than those of the 2-position substituted systems, and their RTP lifetimes are also significantly shorter. Notably, the disubstitution of TA leads to a significant densification of energy level arrangements, thereby substantially increasing the potential ISC channels. Theoretical calculations demonstrate that the energy gaps between S_2 and S_1 for 1TA–BP–1TA and 2TA–BP–2TA were merely 0.01 eV and 0.05 eV, respectively. This small energy difference implies that ISC processes involving the S_2 state cannot be overlooked. Further SOC calculations corroborate this mechanism: strong SOC effects were generally observed between the S_2 state and the T_1–T_{10} states for 1TA–BP–1TA and 2TA–BP–2TA, providing crucial theoretical insights for understanding their highly efficient RTP emission (Fig. S10).

To elucidate the origin of the strong SOC, we performed a systematic natural transition orbital (NTO) analysis for the S_1 and T_1 excited states of 1TA–BP and 2TA–BP, as well as the S_1, S_2, and T_1 excited states of 1TA–BP–1TA and 2TA–BP–2TA (Fig. 3b and Fig. S11–S14). The results reveal that all molecules except the 1TA–BP exhibit similar electronic transition characteristics: their S_1 states consistently show ICT from the non-bonding (n) orbital of the TA sulfur atom to the π orbital of the BP moiety, displaying typical $^1(n, \pi^*)$ transition characteristics. In contrast, the T_1 states are exclusively dominated by π electron localized within the BP fragment, presenting a localized $^3(\pi, \pi^*)$ character. According to El-Sayed's rule, transitions involving a change in orbital type significantly enhance the non-radiative transition (such as ISC) process between excited states of different spin multiplicity.[42] Therefore, the observed $^1(n, \pi^*) \rightarrow {}^3(\pi, \pi^*)$ transition characteristics in this study theoretically provide a good explanation for the mechanism of enhanced SOC and highly efficient ISC in these molecules. However, the situation is different for 1TA–BP, where both its S_1 and T_1 states are predominantly determined by the BP moiety. The strong SOC observed in 1TA–BP can be attributed to the altered orientation of the n orbital on the ketone carbonyl group within BP (Fig. S11). We can also observe this tendency in 1TA–BP–1TA, which could be one of the reasons why the substitution of TA at the 1-position leads to an abrupt increase in SOC between the T_1 and S_0 states (Fig. 3b and Fig. S13).

Benefiting from 2TA–BP–2TA's oxygen-insensitive fluorescence, oxygen-sensitive RTP dual emission, long RTP lifetime, and high ϕ_P, it emerges as a promising candidate material for

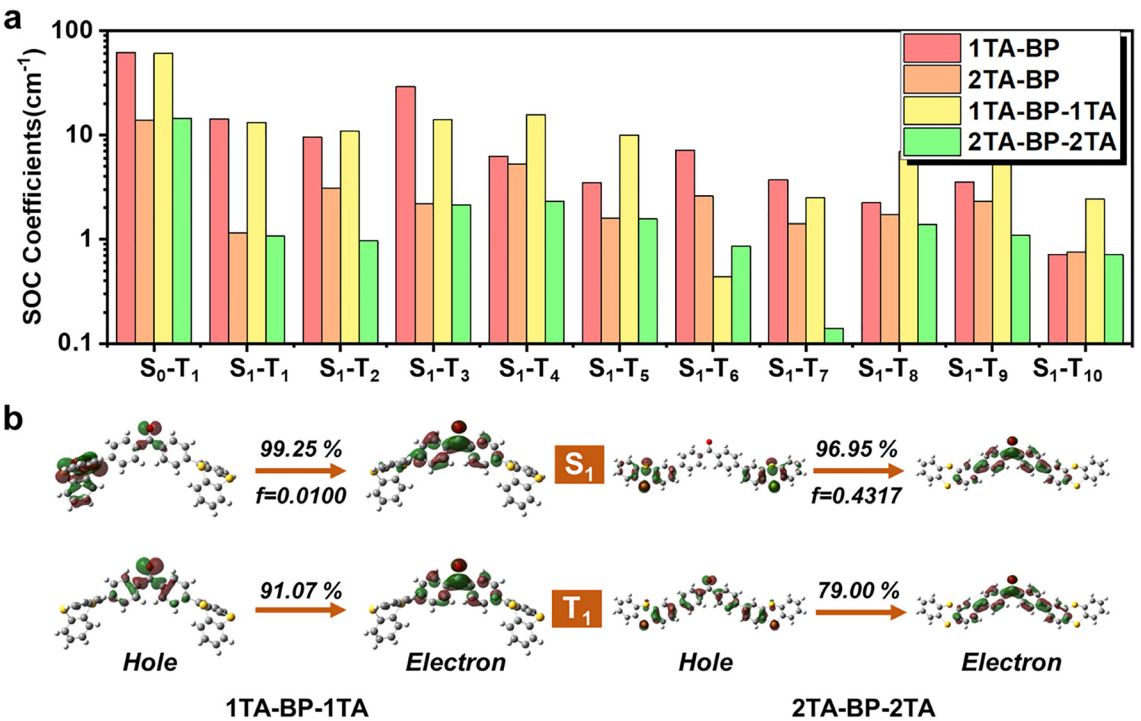

Fig. 3 (a) Comparison of SOC coefficients for 1TA–BP, 2TA–BP, 1TA–BP–1TA, and 2TA–BP–2TA. (b) NTOs of the S_1 and T_1 excited states for 1TA–BP–1TA and 2TA–BP–2TA (only showing orbitals with the most significant contributions; see the SI for details).

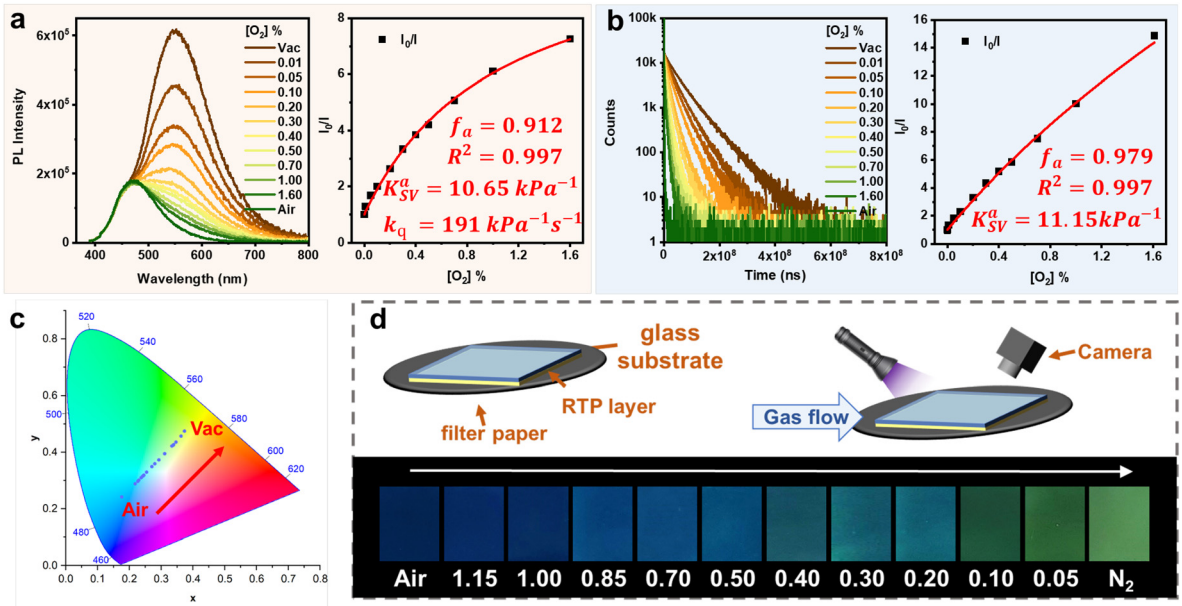

Fig. 4 (a) Steady-state PL spectra and (b) RTP emission decays of 2TA–BP–2TA doped PMMA films under different oxygen conditions, along with the corresponding oxygen sensing performance. (c) CIE coordinates as a function of oxygen concentration derived from the PL spectra. (d) Luminescence photographs under different oxygen concentrations in gas purging and schematic illustration of the photography method.

single-component ratiometric oxygen sensing and detection. To quantitatively measure the oxygen sensitivity of 2TA–BP–2TA, 1.00 wt% doped PMMA films were placed in a nitrogen–oxygen gas mixture containing varying oxygen concentrations, and their PL spectra were recorded *in situ*. As the oxygen concentration increases, its fluorescence emission intensity remains nearly unchanged, while its RTP emission intensity gradually decreases (Fig. 4a). The emission intensity at the fluorescence peak was defined as I_F, and the emission intensity at the RTP peak was defined as I_P. Their ratio, $I = I_P/I_F$ (in the equation, where the subscript '0' denotes the vacuum condition), was then calculated, and a curve showing the relationship between I and the oxygen concentration ($[O_2]$) was plotted. Due to the potential heterogeneity of the doped film, there exist two types of "micro-domains" within it: highly sensitive and lowly sensitive regions. This intrinsic non-uniformity causes the 2TA–BP–2TA doped PMMA films to exhibit a downward-curving plot rather than a linear relationship between I and $[O_2]$. This phenomenon can be described by the modified Stern–Volmer equation proposed by Demas *et al.* (eqn (1)).[43]

$$\frac{I_0}{I} = \frac{\tau_0}{\tau} = \frac{1}{\frac{f_a}{1 + K_{SV}^a[O_2]} + \frac{f_b}{1 + K_{SV}^b[O_2]}} \quad (1)$$

In this equation, K_{SV}^a and K_{SV}^b represent the Stern–Volmer constants for the highly sensitive and lowly sensitive micro-domains, respectively, while f_a and f_b denote the respective fractions of these two micro-domains. The fitting results indicate that its K_{SV}^a reaches an impressive 10.65 kPa^{-1}, and f_a also attains 0.912. This suggests that K_{SV}^a can approximately represent the overall oxygen sensitivity level of the film, a value that surpasses most optical oxygen sensing materials based on purely organic RTP materials.[1,44,45] Based on a 0.1% change in the spectral response, the limit of detection (LOD) is determined to be 0.94 ppm.[1] In addition, the cycling stability and photostability of 2TA–BP–2TA were evaluated. After at least ten air–vacuum cycling processes, the oxygen-sensing performance of the films remained essentially unchanged, indicating reliable cycling stability. Furthermore, after continuous irradiation with intense UV light (4 mW cm^{-2}, 365 nm) for 60 minutes, the ^1H NMR spectra exhibited no significant changes, demonstrating excellent photostability (Fig. S15). Through RTP lifetime measurements under various oxygen concentrations, the kinetic characteristics of its oxygen-quenched RTP were clarified. As the oxygen concentration increases, the RTP lifetime gradually decreases, and a fitted K_{SV}^a value of 11.15 kPa^{-1} with an f_a of 0.979 was obtained (Fig. 4b). These results demonstrate the dynamic quenching nature of oxygen toward the RTP in films. The slightly higher K_{SV} value obtained from lifetime measurements compared to that from PL spectra can be attributed to subtle interference from enhanced RTP intensity on fluorescence under low oxygen concentration conditions.

Furthermore, the significant spectral separation ensures that when the oxygen concentration changes (with fluorescence intensity remaining approximately constant while RTP intensity changes drastically), the emission colour of the thin film will also undergo a substantial alteration. This change is clearly discernible from the CIE coordinates derived from the PL spectra: as the oxygen concentration decreases, the emission colour progressively shifts from a fluorescence-dominated blue to a phosphorescence-dominated yellow-green (Fig. 4c).

Subsequently, by purging the film with nitrogen–oxygen gas mixtures of varying oxygen concentrations, the colour change in the film's emission could be clearly observed by naked eyes (Fig. 4d). As the oxygen concentration in the purging gas decreases, the emission intensity of the thin film gradually increases, and the emission colour progressively transitions from blue to yellow-green. Such distinct differences in both colour and brightness across varying oxygen concentrations highlight its potential as an ''oxygen-sensitive test paper'' for convenient on-site detection.

Conclusions

In conclusion, this work reports a series of purely organic RTP materials with diverse properties by incorporating varying numbers and positions of TA groups with the BP group. It was found that the folded conformation of TA, synergistically with weak ICT, significantly enhances SOC, thereby enabling efficient RTP emission. Through comprehensive experimental and theoretical investigations, despite TA substitution at different positions promoting ISC, the excessively strong SOC induced by 1-position substitution accelerates the non-radiative deactivation of triplet excitons. Consequently, 2-position substitution yields higher RTP efficiency compared to 1-position substitution. Importantly, leveraging the high-efficiency RTP-fluorescence dual emission characteristics and the oxygen sensitivity of the RTP from 2TA–BP–2TA, its successful application in single-component ratiometric oxygen sensing was demonstrated, achieving a remarkable K_{SV} value of up to 10.65 kPa^{-1}. Furthermore, the notable emission color changes of this material under varying oxygen concentrations suggest its potential as an ''oxygen test paper'' for convenient on-site detection of oxygen concentration. This work not only provides a deeper understanding of the structure–property relationship of TA-based purely organic RTP materials but also offers new strategies for their performance optimization and functional development.

Conflicts of interest

There are no conflicts to declare.

Data availability

The data supporting this article have been included as part of the supplementary information (SI). Supporting information: instrumentation details, schematic diagram of the oxygen-dependent spectroscopy setup, synthetic procedures, structural characterization data (including ^{1}H NMR, ^{13}C NMR, and mass spectrometry), additional spectral data, and TD-DFT calculations. See DOI: https://doi.org/10.1039/d5qm00556f.

CCDC 2476748–2476751 contain the supplementary crystallographic data for this paper.[46a–d]

Acknowledgements

This work is supported by the National Natural Science Foundation of China (52373183, 52573196, 52503230, and 52103209), the National Key Research and Development Program of China (No. 2020YFA0714603) and the Postdoctoral Fellowship Program of CPSF (2024M761125 and GZC20250801). We gratefully acknowledge HZWTECH for providing computation facilities.

Notes and references

1 W.-J. Guo, Y.-Z. Chen, C.-H. Tung and L.-Z. Wu, Ultralong Room-Temperature Phosphorescence of Silicon-Based Pure Organic Crystal for Oxygen Sensing, *CCS Chem.*, 2022, **4**, 1007–1015.

2 Z. Yang, J. Qian, S. Zhao, Y. Lv, Z. Feng, S. Wang, H. He, S.-T. Zhang, H. Liu and B. Yang, Highly Sensitive Thianthrene Covalent Trimer Room-Temperature Phosphorescent Materials for Low-Concentration Oxygen Detection, *Angew. Chem., Int. Ed.*, 2025, **64**, e202424669.

3 H. Liu, G. Pan, Z. Yang, Y. Wen, X. Zhang, S.-T. Zhang, W. Li and B. Yang, Dual-Emission of Fluorescence and Room-Temperature Phosphorescence for Ratiometric and Colorimetric Oxygen Sensing and Detection Based on Dispersion of Pure Organic Thianthrene Dimer in Polymer Host, *Adv. Opt. Mater.*, 2022, **10**, 2102814.

4 Y. Fan, Q. Li and Z. Li, Afterglow bio-applications by utilizing triplet excited states of organic materials, *Sci. China: Chem.*, 2023, **66**, 2930–2940.

5 H. Zheng, Z. Zhang, S. Cai, Z. An and W. Huang, Enhancing Purely Organic Room Temperature Phosphorescence via Supramolecular Self-Assembly, *Adv. Mater.*, 2024, **36**, 2311922.

6 H. Jin, X. Jiang, Z. Sun and R. Gui, Phosphorescence-based ratiometric probes: Design, preparation and applications in sensing, imaging and biomedicine therapy, *Coord. Chem. Rev.*, 2021, **431**, 213694.

7 X. Yu, H. Zhang and J. Yu, Luminescence anti-counterfeiting: From elementary to advanced, *Aggregate*, 2021, **2**, 20–34.

8 D. Wang, J. Gong, Y. Xiong, H. Wu, Z. Zhao, D. Wang and B. Z. Tang, Achieving Color-Tunable and Time-Dependent Organic Long Persistent Luminescence via Phosphorescence Energy Transfer for Advanced Anti-Counterfeiting, *Adv. Funct. Mater.*, 2023, **33**, 2208895.

9 Y. Su, Y. Zhang, Z. Wang, W. Gao, P. Jia, D. Zhang, C. Yang, Y. Li and Y. Zhao, Excitation-Dependent Long-Life Luminescent Polymeric Systems under Ambient Conditions, *Angew. Chem., Int. Ed.*, 2020, **59**, 9967–9971.

10 Z. Yang, H. Liu, X. Zhang, Y. Lv, Z. Fu, S. Zhao, M. Liu, S.-T. Zhang and B. Yang, Photo-Responsive Dynamic Organic Room-Temperature Phosphorescence Materials Based on a Functional Unit Combination Strategy, *Adv. Mater.*, 2024, **36**, 2306784.

11 J. Liu, Z.-P. Song, J. Wei, J.-J. Wu, M.-Z. Wang, J.-G. Li, Y. Ma, B.-X. Li, Y.-Q. Lu and Q. Zhao, Circularly Polarized Organic

Ultralong Room-Temperature Phosphorescence with A High Dissymmetry Factor in Chiral Helical Superstructures, *Adv. Mater.*, 2024, **36**, 2306834.
12 L. Li, J. Zhou, J. Han, D. Liu, M. Qi, J. Xu, G. Yin and T. Chen, Finely manipulating room temperature phosphorescence by dynamic lanthanide coordination toward multilevel information security, *Nat. Commun.*, 2024, **15**, 3846.
13 M. Li, Z. Li, X. Peng, D. Liu, Z. Chen, W. Xie, K. Liu and S.-J. Su, Excited-State Engineering of Chalcogen-Bridged Chiral Molecules for Efficient OLEDs with Diverse Luminescence Mechanisms, *Angew. Chem., Int. Ed.*, 2025, **64**, e202420474.
14 S. Zhao, M. Li, Z. Li, Z. Yang, H. He, Y. Lv, M. Yao, B. Li, S.-T. Zhang, H. Liu, S.-J. Su and B. Yang, Efficient Pure Organic Near-Infrared Room-Temperature Phosphorescence Based on n/π Orbital Decoupling, *CCS Chem.*, 2025, DOI: **10.31635/ccschem.025.202405319**.
15 B. Song, W. Shao, J. Jung, S.-J. Yoon and J. Kim, Organic Light-Emitting Diode Employing Metal-Free Organic Phosphor, *ACS Appl. Mater. Interfaces*, 2020, **12**, 6137–6143.
16 G. Baryshnikov, B. Minaev and H. Ågren, Theory and Calculation of the Phosphorescence Phenomenon, *Chem. Rev.*, 2017, **117**, 6500–6537.
17 W. Zhao, Z. He and B. Z. Tang, Room-temperature phosphorescence from organic aggregates, *Nat. Rev. Mater.*, 2020, **5**, 869–885.
18 B. Chang, J. Chen, J. Bao, T. Sun and Z. Cheng, Molecularly Engineered Room-Temperature Phosphorescence for Biomedical Application: From the Visible toward Second Near-Infrared Window, *Chem. Rev.*, 2023, **123**, 13966–14037.
19 G. Yin, J. Zhou, W. Lu, L. Li, D. Liu, M. Qi, B. Z. Tang, P. Théato and T. Chen, Targeting Compact and Ordered Emitters by Supramolecular Dynamic Interactions for High-performance Organic Ambient Phosphorescence, *Adv. Mater.*, 2024, **36**, 2311347.
20 Z. Yang, Z. Fu, H. Liu, M. Wu, N. Li, K. Wang, S.-T. Zhang, B. Zou and B. Yang, Pressure-induced room-temperature phosphorescence enhancement based on purely organic molecules with a folded geometry, *Chem. Sci.*, 2023, **14**, 2640–2645.
21 W. Shao, H. Jiang, R. Ansari, P. M. Zimmerman and J. Kim, Heavy atom oriented orbital angular momentum manipulation in metal-free organic phosphors, *Chem. Sci.*, 2022, **13**, 789–797.
22 H. Li, H. Ma, P. Zhang, Z. An and X. He, Modulating Room-Temperature Phosphorescence of Phenothiazine Dioxide via External Heavy Atoms, *Angew. Chem., Int. Ed.*, 2025, **64**, e202419366.
23 O. Bolton, K. Lee, H.-J. Kim, K. Y. Lin and J. Kim, Activating efficient phosphorescence from purely organic materials by crystal design, *Nat. Chem.*, 2011, **3**, 205–210.
24 Y. Wen, H. Liu, S. Zhang, J. Cao, J. De and B. Yang, Achieving Highly Efficient Pure Organic Single-Molecule White-Light Emitter: The Coenhanced Fluorescence and Phosphorescence Dual Emission by Tailoring Alkoxy Substituents, *Adv. Opt. Mater.*, 2020, **8**, 1901995.
25 Z. Gong, Q. Cui, X. Nie, G. Zhang and B. Chen, Achieving dual-mode long-persistence afterglow through an aromatic furan organic host–guest system, *Mater. Chem. Front.*, 2025, **9**, 676–683.
26 J. Choi, H. Im, J.-M. Heo, D. W. Kim, H. Jiang, A. Stark, W. Shao, P. M. Zimmerman, G. W. Jeon, J.-W. Jang, E. H. Hwang, S. Kim, D. H. Park and J. Kim, Microsecond triplet emission from organic chromophore-transition metal dichalcogenide hybrids *via* through-space spin orbit proximity effect, *Nat. Commun.*, 2024, **15**, 10282.
27 C. A. M. Salla, G. Farias, M. Rouzières, P. Dechambenoit, F. Durola, H. Bock, B. de Souza and I. H. Bechtold, Persistent Solid-State Phosphorescence and Delayed Fluorescence at Room Temperature by a Twisted Hydrocarbon, *Angew. Chem., Int. Ed.*, 2019, **58**, 6982–6986.
28 M. A. Niyas, S. Garain, K. Shoyama and F. Würthner, Room-Temperature Near-Infrared Phosphorescence from C64 Nanographene Tetraimide by π-Stacking Complexation with Platinum Porphyrin, *Angew. Chem., Int. Ed.*, 2024, **63**, e202406353.
29 W. Xu, B. Wang, S. Liu, W. Fang, Q. Jia, J. Liu, C. Bo, X. Yan, Y. Li and L. Chen, Urea-formaldehyde resin room temperature phosphorescent material with ultra-long afterglow and adjustable phosphorescence performance, *Nat. Commun.*, 2024, **15**, 4415.
30 Y. Wen, H. Liu, S.-T. Zhang, G. Pan, Z. Yang, T. Lu, B. Li, J. Cao and B. Yang, Modulating Room Temperature Phosphorescence by Oxidation of Thianthrene to Achieve Pure Organic Single-Molecule White-Light Emission, *CCS Chem.*, 2021, **3**, 1940–1948.
31 N. Li, Y. Wang and Z. Li, Photo-induced room temperature phosphorescence and thermally activated photochromism based on thianthrene derivatives, *J. Mater. Chem. C*, 2024, **12**, 12045–12053.
32 H. Liu, Y. Gao, J. Cao, T. Li, Y. Wen, Y. Ge, L. Zhang, G. Pan, T. Zhou and B. Yang, Efficient room-temperature phosphorescence based on a pure organic sulfur-containing heterocycle: folding-induced spin–orbit coupling enhancement, *Mater. Chem. Front.*, 2018, **2**, 1853–1858.
33 G. Pan, Z. Yang, H. Liu, Y. Wen, X. Zhang, Y. Shen, C. Zhou, S.-T. Zhang and B. Yang, Folding-Induced Spin–Orbit Coupling Enhancement for Efficient Pure Organic Room-Temperature Phosphorescence, *J. Phys. Chem. Lett.*, 2022, **13**, 1563–1570.
34 K. Leitonas, A. Tomkeviciene, G. Baratte, A. Dabuliene, S. M. Punniyakoti, D. Volyniuk and J. V. Grazulevicius, Oxygen sensing properties of thianthrene and phenothiazine derivatives exhibiting room temperature phosphorescence: Effect of substitution of phenothiazine moieties, *Sens. Actuators, B*, 2021, **345**, 130369.
35 X.-d Wang and O. S. Wolfbeis, Optical methods for sensing and imaging oxygen: materials, spectroscopies and applications, *Chem. Soc. Rev.*, 2014, **43**, 3666–3761.
36 Y. Feng, J. Cheng, L. Zhou, X. Zhou and H. Xiang, Ratiometric optical oxygen sensing: a review in respect of material design, *Analyst*, 2012, **137**, 4885–4901.

37 W. Zhao, Z. He, J. W. Y. Lam, Q. Peng, H. Ma, Z. Shuai, G. Bai, J. Hao and B. Z. Tang, Rational Molecular Design for Achieving Persistent and Efficient Pure Organic Room-Temperature Phosphorescence, *Chemistry*, 2016, **1**, 592–602.
38 Y. Su, X. Du, B. Fu, G. Wang, X. Piao, G. Wang and K. Zhang, Disrupting n–π^* Transition of Benzophenone Derivatives' T1 States to Achieve Ultralong-Lived Room-Temperature Phosphorescence, *ACS Mater. Lett.*, 2024, **6**, 1042–1049.
39 W. Luo, Y. Zhang, Y. Gong, Q. Zhou, Y. Zhang and W. Yuan, Crystallization-induced phosphorescence, remarkable mechanochromism, and grinding enhanced emission of benzophenone-aromatic amine conjugates, *Chin. Chem. Lett.*, 2018, **29**, 1533–1536.
40 Z. Feng, Z. Yang, S. Zhao, J. Qian, S.-T. Zhang, H. Liu and B. Yang, Improving Pure Organic Room-Temperature Phosphorescence by Substituent Effect of Thianthrene, *Chin. J. Chem.*, 2025, **43**, 1306–1314.
41 M. Kasha, Characterization of electronic transitions in complex molecules, *Discuss. Faraday Soc.*, 1950, **9**, 14–19.
42 M. A. El-Sayed, Spin—Orbit Coupling and the Radiationless Processes in Nitrogen Heterocyclics, *J. Chem. Phys.*, 1963, **38**, 2834–2838.
43 E. R. Carraway, J. N. Demas, B. A. DeGraff and J. R. Bacon, Photophysics and photochemistry of oxygen sensors based on luminescent transition-metal complexes, *Anal. Chem.*, 1991, **63**, 337–342.
44 S. Wang, H. Shu, X. Han, X. Wu, H. Tong and L. Wang, A highly efficient purely organic room-temperature phosphorescence film based on a selenium-containing emitter for sensitive oxygen detection, *J. Mater. Chem. C*, 2021, **9**, 9907–9913.
45 Z. Cheng, X. Wang, J. Zhao, S. Wang, X. Wu, H. Tong and L. Wang, Efficient Purely Organic Room-Temperature Phosphorescence from Selenium-Containing Conjugated Polymers for Signal-Amplified Oxygen Detection, *Macromolecules*, 2023, **56**, 2972–2979.
46 (*a*) CCDC 2476748: Experimental Crystal Structure Determination, 2025, DOI: **10.5517/ccdc.csd.cc2p4837**; (*b*) CCDC 2476749: Experimental Crystal Structure Determination, 2025, DOI: **10.5517/ccdc.csd.cc2p4848**; (*c*) CCDC 2476750: Experimental Crystal Structure Determination, 2025, DOI: **10.5517/ccdc.csd.cc2p4859**; (*d*) CCDC 2476751: Experimental Crystal Structure Determination, 2025, DOI: **10.5517/ccdc.csd.cc2p486b**.